Multimode phase-matched third-harmonic generation in sub-micrometer-wide anatase TiO_2 waveguides

Christopher C. Evans,[1,3] Katia Shtyrkova,[2] Orad Reshef,[1] Michael Moebius,[1] Jonathan D. B. Bradley,[1,2] Sarah Griesse-Nascimento,[1] Erich Ippen,[2] and Eric Mazur[1,*]

[1]*School of Engineering and Applied Sciences, Harvard University Cambridge, Massachusetts 02138 USA*
[2]*Department of Electrical Engineering and Computer Science, Massachusetts Institute of Technology Cambridge, Massachusetts 02139 USA*
[3]*Current address: Kavli Institute at Cornell for Nanoscale Science, Cornell University Ithaca, New York 14853, USA*
[*]*mazur@seas.harvard.edu*

Abstract: Third-harmonic generation (THG) has applications ranging from wavelength conversion to pulse characterization, and has important implications for quantum sources of entangled photons. However, on-chip THG devices are nearly unexplored because bulk techniques are difficult to adapt to integrated photonic circuits. Using sub-micrometer-wide polycrystalline anatase TiO_2 waveguides, we demonstrate third-harmonic generation on a CMOS-compatible platform. We correlate higher conversion efficiencies with phase-matching between the fundamental pump mode and higher-order signal modes. Using scattered light, we estimate conversion efficiencies as high as 2.5% using femtosecond pulses, and thus demonstrate that multimode TiO_2 waveguides are promising for wideband wavelength conversion and new applications ranging from sensors to triplet-photon sources.

OCIS codes: (190.2620) Harmonic generation and mixing; (130.3130) Integrated optics materials; (190.4390) Nonlinear optics, integrated optics.

References and links

1. T. Alasaarela, L. Karvonen, H. Jussila, A. Säynätjoki, S. Mehravar, R. A. Norwood, N. Peyghambarian, K. Kieu, I. Tittonen, and H. Lipsanen, "High-quality crystallinity controlled ALD TiO_2 for waveguiding applications," Opt. Lett. **38**, 3980–3983 (2013).
2. S. K. Das, C. Schwanke, A. Pfuch, W. Seeber, M. Bock, G. Steinmeyer, T. Elsaesser, and R. Grunwald, "Highly efficient THG in TiO_2 nanolayers for third-order pulse characterization," Opt. Express **19**, 16985–16995 (2011).
3. A. Borne, P. Segonds, B. Boulanger, C. Félix, and J. Debray, "Refractive indices, phase-matching directions and third order nonlinear coefficients of rutile TiO_2 from third harmonic generation," Opt. Mater. Express **2**, 1797–1802 (2012).
4. F. Gravier and B. Boulanger, "Third order frequency generation in TiO_2 rutile and $KTiOPO_4$," Opt. Mater. **30**, 33–36 (2007).
5. M. Furuhashi, M. Fujiwara, T. Ohshiro, M. Tsutsui, K. Matsubara, M. Taniguchi, S. Takeuchi, and T. Kawai, "Development of microfabricated TiO_2 channel waveguides," AIP Adv. **1**, 32102–32105 (2011).

#226754 - $15.00 USD Received 2 Jan 2015; revised 25 Feb 2015; accepted 1 Mar 2015; published 18 Mar 2015

6. M. Furuhashi, M. Fujiwara, T. Ohshiro, K. Matsubara, M. Tsutsui, M. Taniguchi, S. Takeuchi, and T. Kawai, "Embedded TiO_2 waveguides for sensing nanofluorophores in a microfluidic channel," Appl. Phys. Lett. **101**, 153115 (2012).
7. J. T. Choy, J. D. B. Bradley, P. B. Deotare, I. B. Burgess, C. C. Evans, E. Mazur, and M. Lončar, "Integrated TiO_2 resonators for visible photonics," Opt. Lett. **37**, 539–541 (2012).
8. J. D. B. Bradley, C. C. Evans, J. T. Choy, O. Reshef, P. B. Deotare, F. Parsy, K. C. Phillips, M. Lončar, and E. Mazur, "Submicrometer-wide amorphous and polycrystalline anatase TiO_2 waveguides for microphotonic devices," Opt. Express **20**, 23821–23831 (2012).
9. Z.-F. Bi, L. Wang, X.-H. Liu, S.-M. Zhang, M.-M. Dong, Q.-Z. Zhao, X.-L. Wu, and K.-M. Wang, "Optical waveguides in TiO_2 formed by He ion implantation," Opt. Express **20**, 6712–6719 (2012).
10. C. C. Evans, J. D. B. Bradley, E. A. Martí-Panameño, and E. Mazur, "Mixed two- and three-photon absorption in bulk rutile (TiO_2) around 800 nm," Opt. Express **20**, 3118–3128 (2012).
11. C. C. Evans, K. Shtyrkova, J. D. B. Bradley, O. Reshef, E. Ippen, and E. Mazur, "Spectral broadening in anatase titanium dioxide waveguides at telecommunication and near-visible wavelengths," Opt. Express **21**, 18582–18591 (2013).
12. T. Touam, L. Znaidi, D. Vrel, I. Hadjoub, I. N. Kuznetsova, O. Brinza, A. Fischer, and A. Boudrioua, "Low optical loss nano-structured TiO_2 planar waveguides by sol-gel route for photonic crystal applications," Opt. Quant. Electron. **46**, 23–37 (2013).
13. S. Richard, K. Bencheikh, B. Boulanger, and J. A. Levenson, "Semiclassical model of triple photons generation in optical fibers," Opt. Lett. **36**, 3000–3002 (2011).
14. F. Gravier and B. Boulanger, "Cubic parametric frequency generation in rutile single crystal," Opt. Express **14**, 11715–11720 (2006).
15. H. Hübel, D. R. Hamel, A. Fedrizzi, S. Ramelow, K. J. Resch, and T. Jennewein, "Direct generation of photon triplets using cascaded photon-pair sources," Nature **466**, 601–603 (2010).
16. L. K. Shalm, D. R. Hamel, Z. Yan, C. Simon, K. J. Resch, and T. Jennewein, "Three-photon energy-time entanglement," Nature Phys. **9**, 19–22 (2013).
17. D. M. Greenberger, M. A. Horne, A. Shimony, and A. Zeilinger, "Bell's theorem without inequalities," Am. J. Phys. **58**, 1131–1143 (1990).
18. K. Bencheikh, F. Gravier, J. Douady, A. Levenson, and B. Boulanger, "Triple photons: a challenge in nonlinear and quantum optics," C. R. Phys. **8**, 206–220 (2007).
19. T. Hashimoto, T. Yoko, and S. Sakka, "Sol-gel preparation and third-order nonlinear optical properties of TiO_2 thin films," Bull. Chem. Soc. Jpn. **67**, 653–660 (1994).
20. J. S. Levy, M. A. Foster, A. L. Gaeta, and M. Lipson, "Harmonic generation in silicon nitride ring resonators," Opt. Express **19**, 11415–11421 (2011).
21. T. Carmon and K. J. Vahala, "Visible continuous emission from a silica microphotonic device by third-harmonic generation," Nature Phys. **3**, 430–435 (2007).
22. B. Corcoran, C. Monat, C. Grillet, D. J. Moss, B. J. Eggleton, T. P. White, L. O'Faolain, and T. F. Krauss, "Green light emission in silicon through slow-light enhanced third-harmonic generation in photonic-crystal waveguides," Nature Photon. **3**, 206–210 (2009).
23. C. Monat, C. Grillet, B. Corcoran, D. J. Moss, B. J. Eggleton, T. P. White, and T. F. Krauss, "Investigation of phase matching for third-harmonic generation in silicon slow light photonic crystal waveguides using Fourier optics," Opt. Express **18**, 6831–6840 (2010).
24. A. Efimov, A. Taylor, F. Omenetto, J. Knight, W. Wadsworth, and P. Russell, "Phase-matched third harmonic generation in microstructured fibers," Opt. Express **11**, 2567–2576 (2003).
25. We specify height measured by ellipsometry ($\pm$4 nm) and the top-dimension based on the electron-beam mask width.
26. Y. R. Shen, *The Principles of Nonlinear Optics* (John Wiley & Sons, 1984).
27. R. W. Boyd, *Nonlinear Optics* (Academic, 2008).
28. J. A. Armstrong, N. Bloembergen, J. Ducuing, and P. S. Pershan, "Interactions between light waves in a nonlinear dielectric," Phys. Rev. **127**, 1918–1939 (1962).
29. L. Gordon, G. L. Woods, R. C. Eckardt, R. R. Route, R. S. Feigelson, M. M. Fejer, and R. L. Byer, "Diffusion-bonded stacked GaAs for quasi-phase-matched second-harmonic generation of a carbon dioxide laser," Electron. Lett. **29**, 1942 (1993).
30. I. A. Bufetov, M. V. Grekov, K. M. Golant, E. M. Dianov, and R. R. Khrapko, "Ultraviolet-light generation in nitrogen-doped silica fiber," Opt. Lett. **22**, 1394 (1997).
31. A. Zheltikov, "Multimode guided-wave non-3ω third-harmonic generation by ultrashort laser pulses," J. Opt. Soc. Am. B **22**, 2263–2269 (2005).
32. A. M. Zheltikov, "Third-harmonic generation with no signal at 3ω," Phys. Rev. A **72**, 43812 (2005).
33. S. O. Konorov, A. A. Ivanov, M. V. Alfimov, A. B. Fedotov, Y. N. Kondrat'ev, V. S. Shevandin, K. V. Dukel'skii, A. V. Khokhlov, A. A. Podshivalov, A. N. Petrov, D. A. Sidorov-Biryukov, and A. M. Zheltikov, "Generation of frequency-tunable radiation within the wavelength range of 350-600 nm through nonlinear-optical spectral transformation of femtosecond Cr:forsterite-laser pulses in submicron fused silica threads of a microstructure

#226754 - $15.00 USD Received 2 Jan 2015; revised 25 Feb 2015; accepted 1 Mar 2015; published 18 Mar 2015

fiber," Laser Phys. **13**, 1170–1174 (2003).
34. M. Corona, K. Garay-Palmett, and A. B. U'Ren, "Experimental proposal for the generation of entangled photon triplets by third-order spontaneous parametric downconversion in optical fibers," Opt. Lett. **36**, 190–192 (2011).
35. M. Corona, K. Garay-Palmett, and A. B. URen, "Third-order spontaneous parametric down-conversion in thin optical fibers as a photon-triplet source," Phys. Rev. A **84**, 33823 (2011).
36. R. G. Hunsperger, *Integrated Optics: Theory and Technology* (Springer, 2009).
37. M. Levenson and N. Bloembergen, "Dispersion of the nonlinear optical susceptibility tensor in centrosymmetric media," Phys. Rev. B **10**, 4447–4463 (1974).
38. A. M. Armani, R. P. Kulkarni, S. E. Fraser, R. C. Flagan, and K. J. Vahala, "Label-free, single-molecule detection with optical microcavities," Science **317**, 783–787 (2007).
39. S. Arnold, M. Khoshsima, I. Teraoka, S. Holler, and F. Vollmer, "Shift of whispering-gallery modes in microspheres by protein adsorption," Opt. Lett. **28**, 272–274 (2003).
40. F. Vollmer and S. Arnold, "Whispering-gallery-mode biosensing: label-free detection down to single molecules," Nat. Methods **5**, 591–596 (2008).
41. M. D. Baaske, M. R. Foreman, and F. Vollmer, "Single-molecule nucleic acid interactions monitored on a label-free microcavity biosensor platform," Nat. Nanotechnol. **9**, 933–939 (2014).

1. Introduction

Titanium dioxide (TiO_2) is a wide bandgap semiconductor (3.1 eV) with high linear and nonlinear refractive indices, and strong birefringence. These properties make TiO_2 attractive for wavelength conversion using third-harmonic generation (THG) [1–4], integrated optics applications [1, 5–12], and as a promising source of entangled triplet photons [3, 4, 13, 14] for quantum information applications [15, 16]. This final application is of particular importance, because an efficient direct source of continuous-variable Greenberger-Horne-Zeilinger (GHZ) [17] photons has been elusive so far [18]. THG has been explored in both bulk [3, 4, 14] and thin films of TiO_2 [1, 2, 19]. On the other hand, demonstrations of THG using integrated waveguide-based devices have been limited to silicon nitride resonators [20], silica microtoroids [21], and silicon photonic crystals [22, 23]. Achieving phase-matching for efficient THG is a challenge for such waveguide-based devices, requiring careful design and fabrication [23, 24]. To highlight this challenge, and how it can be overcome in our TiO_2 platform, we show an optical image of the green light generation in an anatase TiO_2 waveguide (255 nm high, 800 nm wide [25]) when pumping with femtosecond pulses at 1565 nm in Fig. 1 (left). We see that the strong green-light spectrum appears at 534 nm in Fig. 1 (right) and not at one-third of the central pump wavelength (522 nm). This apparent signal-shift is a consequence of waveguide-based phase-matching that we will explore throughout this paper.

We characterize THG of femtosecond pulses in polycrystalline anatase integrated optical waveguides in three experiments. (1) We confirm THG by measuring scattered green light as a function of propagation distance when pumped using 1550-nm light, and use this to estimate the THG efficiency. (2) We compare the THG signal from waveguides having phase-matched and non-phase-matched geometries at a fixed pump wavelength. (3) We observe changes in THG signal within a single waveguide when sweeping the pump wavelength. Our experiments demonstrate nanoscale-feature-size dependence of the THG signal and strong THG using multimode (MM) phase matching in TiO_2 waveguides.

2. Background theory

In third-harmonic generation, three pump photons (*e.g.*, around $\lambda_p = 1500$ nm) are simultaneously annihilated via a $\chi^{(3)}$-process to produce one signal photon (*e.g.*, around $\lambda_s = 500$ nm). This process requires high pump intensities as $I_s \propto I_p^3$ (signal and pump intensities, respectively). Furthermore, we must conserve both photon energy and momentum for high efficiency. Optimizing this process requires minimizing the phase mismatch between these two wavelengths. For the degenerate pump case, critical-phase-matching requires matching the effective

#226754 - $15.00 USD Received 2 Jan 2015; revised 25 Feb 2015; accepted 1 Mar 2015; published 18 Mar 2015

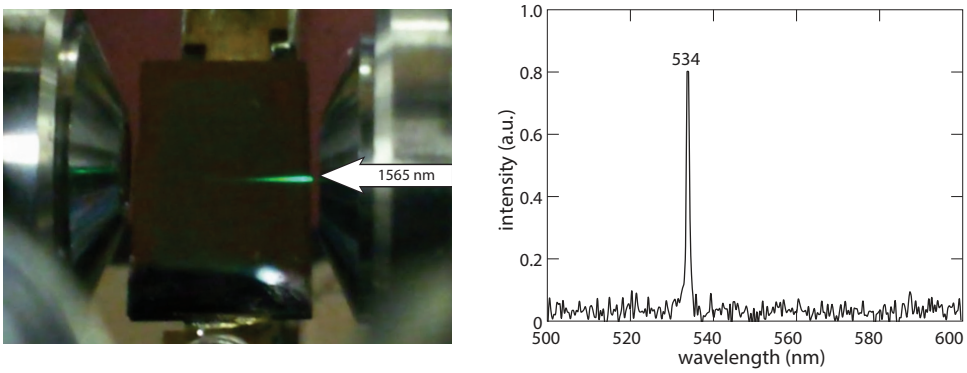

Fig. 1. Green light generation in a polycrystalline anatase TiO_2 waveguide using a 1565-nm pump: top-view optical image of the chip (left) and corresponding visible spectrum (right). The observed peak around 534 nm is shifted from the expected third-harmonic signal predicted if we consider energy conservation alone (521.7 nm).

indices of refraction, $n_p(\lambda_p) = n_s(\lambda_p/3)$, and is the central problem when engineering THG. Here, $n_p(\lambda)$ and $n_s(\lambda)$ are the effective indices experienced by the pump and signal, respectively, and λ_p is the central pump wavelength at the phase-matching point. For most optical materials, the index of refraction decreases with increasing wavelength, making critical-phase-matching difficult or impossible for such widely spaced wavelengths.

This problem is especially difficult for integrated optical devices. Common techniques for circumventing this dispersion in bulk materials, such as birefringence [26, 27], and quasi phase matching [28,29] require epitaxially-grown films or special layered materials (respectively) that we cannot easily apply to integrated optical formats. Furthermore, within a single waveguide mode, the field at shorter signal wavelengths is more strongly confined than at longer pump wavelengths, creating strong waveguide dispersion. The compounded effects of material and waveguide dispersion necessitate a novel approach applicable to integrated waveguides.

Multi-mode (MM) dielectric waveguides provide such an alternative method for phase-matching between widely separated wavelengths. This technique was first discovered in doped silica fiber [30] and was later applied to photonic crystal fiber [31–33] as well as several other integrated optical formats [20–22]. As higher-order modes approach the long-wavelength cut-off, their effective indices decrease more rapidly than for the fundamental modes due to their increased evanescent wave components. This rapid decrease allows us to match effective indices between fundamental (pump) and higher-order (signal) modes, even across one-and-a-half octaves. This technique can greatly increase conversion efficiency, provided there is high field overlap between the pump and signal modes. Therefore, by designing MM waveguides, we can engineer mode-pairs for specific THG wavelengths with greater wavelength flexibility than traditional phase-matching approaches.

Theory predicts several distinctive features indicative of phase-matched THG in MM waveguides that we can use to design and guide our analysis. For reference, we consider the case without phase matching. Consider the pump spectrum, $I_p(\lambda)$, and the energy-shifted pump (ESP) spectrum, given by $I_p(\lambda/3)$. In the absence of phase matching, the three-photon correlation function should produce THG signal that is wider than the ESP spectrum. This is very different for the MM phase-matched case. To gain physical intuition into this effect, we observe that the higher-order modes strong decrease in effective index implies very different group velocities for the pump and signal at the crossing point, where $n_p(\lambda_p) = n_s(\lambda_p/3)$, limiting the phase-matched bandwidth. Neglecting self-phase modulation, this angular frequency bandwidth is

#226754 - $15.00 USD Received 2 Jan 2015; revised 25 Feb 2015; accepted 1 Mar 2015; published 18 Mar 2015

given by $\Delta\omega \approx 2\pi/(|v_s^{-1} - v_p^{-1}|z)$ where v_s and v_p are the group velocities at the signal and pump wavelengths, respectively, and z is the propagation length within the waveguide [31, 32]. Considering femtosecond pulses and effective propagation distances on the order of 1 mm, the bandwidth of THG can be significantly different from the ESP spectrum, from which we expect three features to be evident. First, the conversion should occur over longer distances and with higher efficiency than could occur without phase matching. Second, the signal spectrum may be significantly narrower than the ESP spectrum because of limited phase-matching bandwidth. Third, the phase-matching condition may select out a portion of the ESP spectrum, potentially offsetting the signal from the center of the ESP spectrum.

3. Experiment

3.1. Efficiency of scattered third-harmonic light

We observe the decay of scattered green-signal light (I_{sig}) as a function of distance to test for the cubic dependence of the THG signal relative to the pump. We utilize polycrystalline anatase TiO_2 strip-waveguides fabricated using reactive sputtering and electron-beam lithography on silicon substrates, as described by Bradley *et al.* [8]. The bottom cladding is SiO_2 (thermal oxide) and the top cladding is SiO_2, deposited using chemical vapor deposition. Here, we measured the intensity decay in a 255-nm thick and 280-nm wide (top width) waveguide, with a sidewall angle of 75°(Fig. 2, inset). We excite the fundamental transverse-electric (TE) mode of our waveguides using a Ti:Sapphire-pumped optical parametric oscillator tuned to a central wavelength of 1550 nm. This laser produces 180-fs pulses at 80 MHz with up to 360 mW of average power. No dispersion compensation is applied. We measure the scattered green signal (I_{sig}, with an observed peak wavelength of 515 nm) using a 0.28-NA collection objective that images our waveguides on a CCD camera. We calibrate the CCD camera using a separate 520-nm source. Figure 2 shows the scattered green-light intensity as a function of distance along the waveguide when pumped with 85 mW of average power (measured before the objective). The intensity variations correspond to scattering centers we observe at both visible and infrared wavelengths. To understand the behavior of the observed signal, we present the measured intensity decay for the pump itself at 1550 nm (I_{IR}) and for a 520-nm reference (I_{vis}), when injected during separate experiments. In addition, we plot the cube of the infrared 1550 nm peak intensity (I_{IR}^3), when taking both loss and dispersion into account to model the THG signal.

Comparing the decay of I_{sig} with I_{vis}, we find the decay rate for the reference green light (I_{vis}) is much higher than that for the generated green light (I_{sig}). Therefore, it is evident that the green signal is being re-generated along the waveguide. Meanwhile, we find that I_{IR}^3 fits the data well. The observed generated-green signal has a bandwidth of 3.4 nm. This bandwidth corresponds to an effective phase-matched interaction length of 60 μm. This length is shorter than the visible streak, consistent with scattering centers interrupting signal buildup. We observe that the infrared pump generates green light continuously along the waveguide proportional to the cube of the infrared intensity, and we therefore conclude that the signal is due to THG.

To estimate the efficiency of scattered green light emission, we integrate I_{sig} from the top view camera images and compare to our injected pump power. We collect 6.6 μW of scattered light vertically along the waveguide through a compound microscope when pumping using 62 mW at 1550 nm (measured after the coupling objective). Accounting for our collection efficiency using a 0.28-NA objective (a solid angle of 0.25 sr) and assuming that scattering occurs equally throughout a hemisphere (2π sr, conservatively assuming a perfect reflection from the substrate), our scaled scattered power totals 165 μW. Using a measured coupling coefficient of 10 ± 1 dB/facet at 1550 nm (the largest source of error), we estimate a conversion efficiency to scattered light of $2.5 \pm 0.5\%$. In comparison, collinear bulk rutile measurements

#226754 - $15.00 USD Received 2 Jan 2015; revised 25 Feb 2015; accepted 1 Mar 2015; published 18 Mar 2015

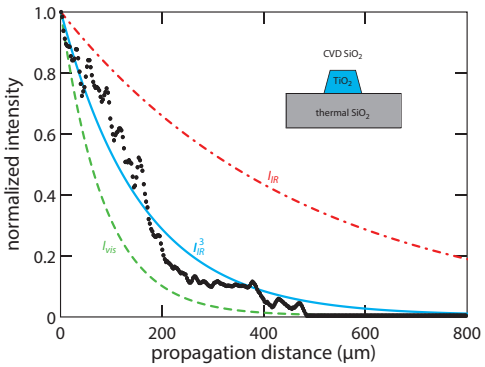

Fig. 2. Normalized scattered visible light intensity (I_{sig}, 509 nm) as a function of propagation distance (black circles) for the waveguide cross section shown in the inset. Comparing the decay of the observed signal to separately measured visible intensity (I_{vis}, 520 nm, dashed green), infrared intensity (I_{IR}, 1550 nm, dash-dot red), and the cubed infrared intensity (I_{IR}^3, solid blue), we infer that the visible light we observe is third-harmonic signal generated within the waveguide.

have yielded an efficiency of 1.3% at 617 nm for a peak pump intensity of 7.4 MW/cm^2 [3].

3.2. Geometry-dependent third-harmonic generation

In the second experiment, we compare the visible-light generation in TiO_2 waveguides with different widths and using a fixed pump wavelength. We use two polycrystalline TiO_2 waveguides that are 255-nm thick, and 700-nm and 900-nm wide (top widths), respectively, both of which have a fluoropolymer top cladding. For each waveguide, we inject 330 mW of 1550-nm pump power and collect the generated visible light using an out-of-plane multimode fiber placed in close proximity to the waveguide. We adjust the fiber placement to maximize signal and then record each spectrum using a spectrometer. Because the coupling, chip, and fiber placement varies for each measurement, the visible signal strength only qualitatively indicates relative THG efficiency.

We observe different THG behavior in each waveguide. The signal-spectra generated for a 1550-nm pump wavelength in waveguides with nominal widths of 700 nm and 900 nm are shown in Fig. 3 (left and right, respectively). In the same figure, we show spectra from an additional 900-nm wide waveguide (right, blue line) fabricated on the same chip. For the 700-nm wide waveguide, the signal is very low and close to the noise floor of the spectrometer. Upon visual inspection of the chip, we observe dramatically less generated green light. Additionally, the THG spectrum is only slightly narrower than the ESP spectrum. Meanwhile, waveguides designed to be 900-nm wide show a bright streak of green light, similar to that in Fig. 1. The visible signal has peaks around 521.8 nm and 526.8 nm in the first and second waveguide, respectively, and are an order of magnitude stronger than for the 700-nm waveguide. Additionally, these spectra do not resemble the ESP spectrum in terms of central wavelength or spectral width. We note that both signal-spectra are at the red edge of, but within, the ESP spectrum. The signal strength, bandwidth, and central wavelength are significantly different for 700-nm versus 900-nm wide waveguides, implying different THG mechanisms at work.

Self-phase modulation adds an additional term to the phase-mismatch calculation, shifting the THG spectrum with sufficient intensity, and is the source of spectral broadening, which increases the pumps bandwidth. To explore this effect in our waveguides, we reduce the average pump power from 330 mW to 200 mW. We do not observe a change in the THG spectrum,

#226754 - $15.00 USD Received 2 Jan 2015; revised 25 Feb 2015; accepted 1 Mar 2015; published 18 Mar 2015

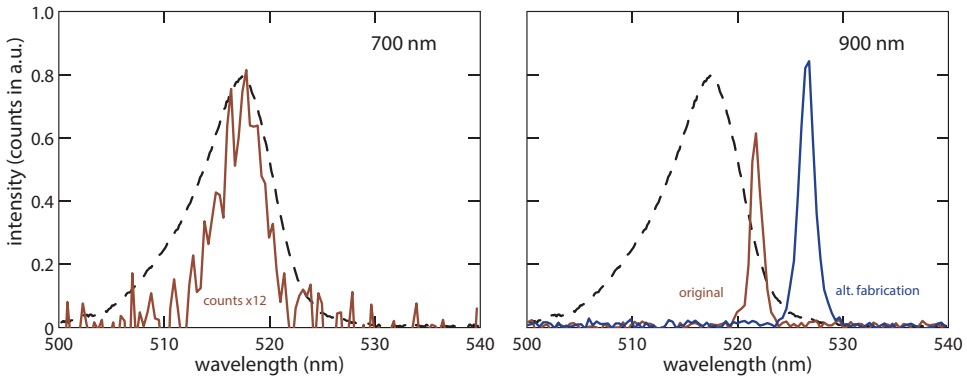

Fig. 3. Visible spectra for different waveguide dimensions showing phase-matched and non-phase-matched conditions. We show the energy-shifted pump spectrum, $I_p(3\lambda)$, as a dashed line. The signal from the 700-nm wide waveguide is weak with a poor signal-to-noise ratio (red curve) and follows the energy-shifted pump spectrum, consistent with non-phase-matched THG. Meanwhile, the 900-nm wide waveguides generate strong, narrow-bandwidth signal offset from the central energy-shifted pump wavelength. From simulation, we infer that the differences between the two 900-nm wide signals (red and blue) are likely due to a 2% fabrication variation.

although we continue to observe spectral broadening of the pump [11]. Therefore, we neglect the self-phase modulation term in our phase-matching analysis, yet consider the effects of a spectrally-broadened pump.

We broadly categorize the markedly different behaviors between waveguides of different dimensions as phase matched and non-phase matched. The weak, broad signal that follows the ESP spectrum for the 700-nm wide waveguide is consistent with non-phase-matched THG. On the other hand, the 900-nm wide waveguides show strong, narrow signal that is within the ESP bandwidth with a shifted central wavelength. Although the 526.8-nm peak is shifted near the red edge of the ESPs bandwidth, this peak falls within an ESP spectrum that is spectrally broadened with SPM and intrapulse Raman scattering [11]. The increased efficiency, decreased bandwidth, and wavelength offset we observe in the 900-nm wide waveguides suggest that only these waveguides achieve MM phase matching around 1550 nm.

To confirm the source of these drastically different THG signals, we compare our data to simulation. We calculate the total dispersion, $\beta(\lambda)$, for all guided modes from 500 nm to the cutoff condition using a commercial finite-difference eigenmode solver. Figure 4 shows the effective index versus pump and signal wavelength for the fundamental and several higher-order modes, respectively. For each pair of modes, we calculate the phase-matched wavelength (PMW), corresponding to $\lambda_s = \lambda_p/3$, shown as a crossing in the figure. In addition, we calculate the pump-signal overlap and denote modes with numerically-zero overlap using a dashed line in Fig. 4 [34, 35]. For simplicity, we focus on two mode-pairs having PMWs closest to the ESP central wavelength. The 700-nm wide waveguide displays PMWs of 502.7 nm (zero overlap) and 540.4 nm (non-zero overlap), falling to the blue edge and outside of the ESP spectrum, respectively. The absence of PMWs with non-zero overlap within the ESP spectrum explains the lack of characteristic phase-matched THG signal. On the other hand, the 900-nm wide waveguide has calculated PMWs at 521.7 nm (zero overlap) and 528.8 nm (non-zero overlap), both within the spectrally-broadened ESP spectrum. These PMWs are similar to our observed signals around 521.8 and 526.8 nm, however, we note that we were unable to observe two visible peaks simultaneously, consistent with overlap analysis. Our simulations reveal that the

#226754 - $15.00 USD Received 2 Jan 2015; revised 25 Feb 2015; accepted 1 Mar 2015; published 18 Mar 2015

green-light signal we observe in 900-nm versus 700-nm wide waveguides directly corresponds to the availability of PMWs with non-zero overlap within the ESP spectrum.

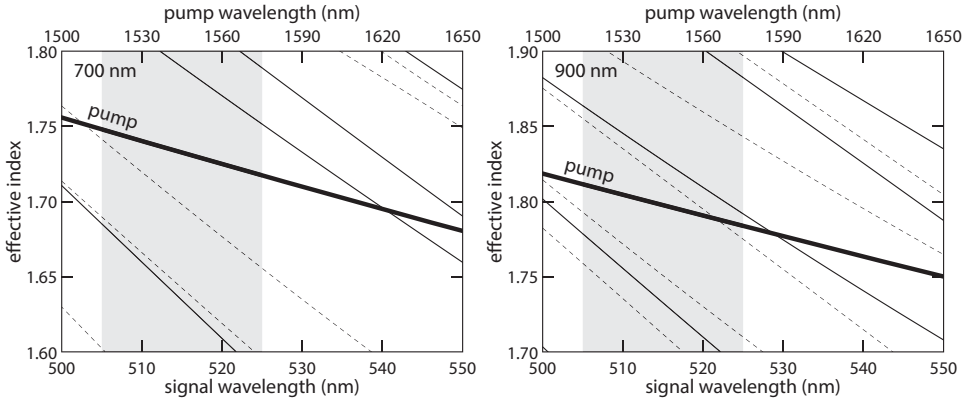

Fig. 4. Calculated effective index versus wavelength for several signal-modes (thin lines, bottom labels) around 525 nm for 700- and 900-nm wide waveguides. In addition, we show the energy-shifted pump-mode (thick lines, top labels). Dashed lines denote modes with numerically-zero pump-signal overlap, and the grayed-area shows the ESP bandwidth. A PMW appears as a crossing between the pump and signal lines in this plot. The 700-nm wide waveguide has a PMW with non-zero overlap far outside of the ESP-spectrum while the 900-nm wide waveguide displays a PMW with non-zero overlap slightly red-shifted from the ESP-spectrum.

3.3. Wavelength-dependent third-harmonic generation

In the third experiment, we observe THG as a function of pump wavelength in a single waveguide. To reduce the number of PMWs, we investigate a waveguide with a smaller cross section, having fewer higher-order modes at visible wavelengths, specifically, a 255-nm thick, 280-nm wide waveguide, similar to the one used in the first experiment. Based on simulations, this waveguide has a single, isolated PMW with non-zero pump-signal overlap [36] around 510 nm. We tune the central pump wavelength from 1440–1560 nm in 10-nm steps and observe visible light generated using 20 mW of average pump power. Over this tuning range, our pump laser bandwidth varies from 10–31 nm, which corresponds to transform-limited pulse durations between 110–310 fs. This configuration allows us to isolate a single PMW and observe how it varies with pump wavelength.

In Fig. 5 we show each spectrum as an intensity plot for each pump wavelength, allowing us to explore the pump wavelength-dependence near a single PMW. For clarity, we denote the peak of each spectrum with a circle and show the ESP central wavelength as a solid line. We observe three key features. First, the signal closely follows the ESP-line ($\lambda_s = \lambda_p/3$) for wavelengths shorter than 1500 nm. Second, we observe strong signal when pumping between 1500 nm and 1550 nm. Third, the signal crosses the ESP-line around 1530 nm, and is comparatively insensitive to pump wavelength at nearby wavelengths, both in terms of peak-wavelength and intensity. Specifically, the variation in the visible-wavelength peaks between pump wavelengths from 1510–1550 nm spans 4 nm, whereas the ESP-line spans over 13 nm. Scanning across a known PMW shows how geometry strongly dictates the strength and shape of the visible spectrum.

This experiment allows us to observe both phase-matched and non-phase-matched conditions within the same waveguide. Between 1510–1550 nm, we attribute the strong signal and the shift

#226754 - $15.00 USD Received 2 Jan 2015; revised 25 Feb 2015; accepted 1 Mar 2015; published 18 Mar 2015

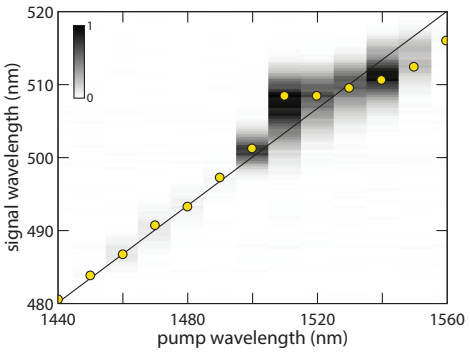

Fig. 5. Visible spectra as a function of pump wavelength for a 280-nm wide waveguide. For each pump wavelength, we show the corresponding visible spectrum vertically as an intensity plot, and we mark the peak wavelength with a yellow circle. For reference, the energy-conservation line ($\lambda_s = \lambda_p/3$, energy-shifted pump line) is shown as a solid line. Between 1440 and 1490 nm, the signal is weak and follows the energy-shifted pump line. Around 1520 nm, the visible signal around 509 nm is much stronger and varies little with pump wavelength, signifying phase-matched third-harmonic generation.

away from the ESP-line to MM phase matching. This shift suggests a PMW of 509 nm, which is very close to our calculated PMW of 510 nm. Second, the weak signal we observe from 1440–1490 nm closely follows the ESP-line, which is consistent with non-phase-matched THG. Longer transform-limited pulse durations at shorter wavelengths and uncompensated dispersion may play a role in the decreased efficiency. We are unable to draw conclusions from the abrupt shift in signal wavelength (slightly shifted from the ESP-line) and strong signal around 1500 nm as it does not correspond to a calculated PMW. Finally, we expect that tuning over a wider range should produce additional phase-matched wavelengths. The signal strengths and offsets demonstrate both non-phase-matched and phase-matched wavelengths within the same TiO_2 waveguide.

4. Discussion

Our experiments demonstrate how engineering submicrometer-wide TiO_2 waveguide dimensions can increase THG efficiency and provide a means to select PMWs. By optimizing the waveguide geometry to take advantage of near-cutoff dispersion, it is possible to engineer modal-pairs to enhance THG across a wider range of wavelengths than is possible considering birefringence in the bulk material alone. For example, birefringent phase-matching in rutile TiO_2 is limited to signal wavelengths longer than 612 nm [3]. The shortest wavelength we demonstrate here, 509 nm, is by no means a fundamental limit. Removing this wavelength constraint will enable direct triplet photons in the C-band (*i.e.*, the down-conversion of a 500-nm pump photon to three 1500-nm photons), which is advantageous for long-range secure quantum communication. In future devices, exploring methods to reduce scattering losses at visible wavelengths will be necessary to enable THG extraction and boost conversion efficiency. In addition to increased wavelength flexibility, this MM phase-matching approach promises to significantly boost triplet generation rates to practical levels [34, 35].

Analyzing the variation in 900-nm-wide waveguide signals demonstrates that strict dimensional tolerances are required for THG bandwidth tuning, and imply that we can use the interplay between phase-matching and pump-signal overlap to enhance THG efficiency. From our data alone, it is unclear whether we are observing two separate mode-pairs or a single

#226754 - $15.00 USD Received 2 Jan 2015; revised 25 Feb 2015; accepted 1 Mar 2015; published 18 Mar 2015

mode-pair with a shifted PMW due to dimension variations from fabrication. Variations as small as 2% in simulations can shift the PMW by over 3 nm, implying that strict tolerances may be required for most applications. We suspect that a single, dominant PMW is present and shifts from fabrication variations for two reasons: first, we did not observe two simultaneous peaks and second, the pump-signal overlap is numerically zero for our calculated 521.7 PMW. In addition to optimizing pump-signal overlap, using co-polarized pump and signal modes, which access larger $\chi^{(3)}$-tensor elements, should increase efficiency [27, 37]. Therefore, future research should explore how waveguide geometry can decrease fabrication sensitivity while simultaneously optimizing overlap and polarization to increase efficiency.

5. Conclusion

We have demonstrated phase-matched THG from telecommunication to visible wavelengths in polycrystalline anatase TiO_2 waveguides, opening the door for applications in telecommunications, sensing, and quantum information. THG provides a method to convert C-band telecommunications signals to visible wavelengths for detection using inexpensive silicon detectors or for visible photonic applications. In particular, the reduced bandwidth and comparative insensitivity to pump wavelength may have applications in wavelength division multiplexing. We can exploit the strong sensitivity of THG to waveguide properties as a novel adsorption-based sensor for chemical and bio-sensing [38–41]. In addition, strong THG implies that third-order parametric down-conversion may be possible to create an efficient source of photon triplets, which has important implications for quantum information applications [15, 16, 18, 34, 35].

Funding information

National Science Foundation (NSF) (ECCS 0901469, ECCS-1201976); Air Force Office of Scientific Research (AFOSR) (FA9550-12-0499, FA9550-11-C-0028); National Science Foundation Graduate Research Fellowship Program (NSFGRFP) (DGE1144152); National Defense Science and Engineering Graduate (NDSEG) Fellowship (32 CFR 168a); Harvard Quantum Optics Center (HQOC) Graduate Student Fellowship; Natural Sciences and Research Council (NSERC) of Canada; Harvard Graduate Prize Fellowship.

Acknowledgments

Several people contributed to the work described in this paper. C.E. and K.S. conceived of the basic idea for this work. O.R. and J.B. fabricated the waveguides. C.E. and K.S. performed measurements. C.E., M.M., O.R., and S.G.-N. performed the simulations. E.M. and E.I. supervised the research and the development of the manuscript. C.E. wrote the first draft of the manuscript; all authors subsequently took part in the revision process and approved the final copy of the manuscript. Philip Muñoz and Nabiha Saklayen provided feedback on the manuscript throughout its development. The authors would also like to acknowledge the use of facilities of the Center for Nanoscale Systems at Harvard University, which is supported by the National Science Foundations National Nanotechnology Infrastructure Network.

#226754 - $15.00 USD Received 2 Jan 2015; revised 25 Feb 2015; accepted 1 Mar 2015; published 18 Mar 2015